NAVAL POSTGRADUATE SCHOOL
Monterey, California

THESIS

SEA SURFACE CURRENT ESTIMATES OFF CENTRAL CALIFORNIA AS DERIVED FROM ENHANCED AVHRR INFRARED IMAGES

by

Fang, Chung-Ming

September 1987

Co-Advisor Steven R. Ramp
Co-Advisor Philip A. Durkee

Approved for public release; distribution is unlimited.

SECURITY CLASSIFICATION OF THIS PAGE

REPORT DOCUMENTATION PAGE

1a REPORT SECURITY CLASSIFICATION UNCLASSIFIED	1b RESTRICTIVE MARKINGS
2a SECURITY CLASSIFICATION AUTHORITY	3 DISTRIBUTION / AVAILABILITY OF REPORT APPROVED FOR PUBLIC RELEASE; DISTRIBUTION IS UNLIMITED.
2b DECLASSIFICATION / DOWNGRADING SCHEDULE	
4 PERFORMING ORGANIZATION REPORT NUMBER(S)	5 MONITORING ORGANIZATION REPORT NUMBER(S)
6a NAME OF PERFORMING ORGANIZATION NAVAL POSTGRADUATE SCHOOL 6b OFFICE SYMBOL (If applicable) CODE 68	7a NAME OF MONITORING ORGANIZATION NAVAL POSTGRADUATE SCHOOL
6c ADDRESS (City, State, and ZIP Code) MONTEREY, CALIFORNIA 93943-5000	7b ADDRESS (City, State, and ZIP Code) MONTEREY, CALIFORNIA 93943-5000
8a NAME OF FUNDING / SPONSORING ORGANIZATION 8b OFFICE SYMBOL (If applicable)	9 PROCUREMENT INSTRUMENT IDENTIFICATION NUMBER
8c ADDRESS (City, State, and ZIP Code)	10 SOURCE OF FUNDING NUMBERS PROGRAM ELEMENT NO / PROJECT NO / TASK NO / WORK UNIT ACCESSION NO

11 TITLE (Include Security Classification)
SEA SURFACE CURRENT ESTIMATES OFF CENTRAL CALIFORNIA AS DERIVED FROM ENHANCED AVHRR INFRARED IMAGES.

12 PERSONAL AUTHOR(S) FANG, CHUNG-MING

13a TYPE OF REPORT	13b TIME COVERED	14 DATE OF REPORT (Year Month Day)	15 PAGE COUNT
MASTER'S THESIS	FROM ____ TO ____	1987, SEPTEMBER	51

16 SUPPLEMENTARY NOTATION

17 COSATI CODES			18 SUBJECT TERMS (Continue on reverse if necessary and identify by block number)
FIELD	GROUP	SUB-GROUP	REMOTE SENSING, IMAGE PROCESSING, OCEAN CURRENTS, FEATURE TRACKING TECHNIQUES.

19 ABSTRACT (Continue on reverse if necessary and identify by block number)

A technique is presented which uses an interactive computer program to estimate sea surface current velocities from the displacement of sea surface temperature (SST) patterns apparent in enhanced sequential Infrared (IR) images obtained from the NOAA-6 Advanced Very High Resolution Radiometer (AVHRR). This technique was applied to the surface currents of the California Current System using IR image data from 27 and 28 April 1981. This technique, which uses enhanced pseudocolor gradient imagery, produced more current vectors than an earlier technique developed by O'Hara (1987) which used unenhanced gray scale imagery. The resultant surface vectors agree well in direction but underestimate velocities obtained from Doppler Acoustic Log (DAL) measurements taken during the same period. The two methods produced closest agreement for current velocities of less than 40 cm/sec and with satellite-derived velocities obtained with sequential 12 hour images rather than sequential 24 hour images. Satellite-derived velocities in the rapid flow area (larger than 40 cm/sec) showed poor correspondence to DAL-measured velocities. The strong current shear in these areas may distort the surface SST patterns making identification of features between two images more difficult. The satellite derived surface velocities are assumed to be representative of the velocities of the upper mixed layer, which is usually 10 to 30 m deep in the study region.

20 DISTRIBUTION / AVAILABILITY OF ABSTRACT	21 ABSTRACT SECURITY CLASSIFICATION
☒ UNCLASSIFIED/UNLIMITED ☐ SAME AS RPT ☐ DTIC USERS	UNCLASSIFIED

22a NAME OF RESPONSIBLE INDIVIDUAL	22b TELEPHONE (Include Area Code)	22c OFFICE SYMBOL
STEVEN R. RAMP, Assistant Professor	(408) 646-3162	CODE, 68 Ra

DD FORM 1473, 84 MAR — 83 APR edition may be used until exhausted. All other editions are obsolete.

SECURITY CLASSIFICATION OF THIS PAGE
UNCLASSIFIED

Approved for public release; distribution is unlimited.

Sea Surface Current Estimates off Central California as Derived from Enhanced AVHRR Infrared Images

by

Fang, Chung-Ming
Lieutenant Commander, Taiwan R.O.C Navy
B.S., Cheng-Chung Institute of Technology (Taiwan 1979)

Submitted in partial fulfillment of the
requirements for the degree of

MASTER OF SCIENCE IN OCEANOGRAPHY

from the

NAVAL POSTGRADUATE SCHOOL
September 1987

ABSTRACT

A technique is presented which uses an interactive computer program to estimate sea surface current velocities from the displacement of sea surface temperature (SST) patterns apparent in enhanced sequential Infrared (IR) images obtained from the NOAA-6 Advanced Very High Resolution Radiometer (AVHRR). This technique was applied to the surface currents of the California Current System using IR image data from 27 and 28 April 1981. This technique, which uses enhanced pseudocolor gradient imagery, produced more current vectors than an earlier technique developed by O'Hara (1987) which used unenhanced gray scale imagery. The resultant surface vectors agree well in direction but underestimate velocities obtained from Doppler Acoustic Log (DAL) measurements taken during the same period. The two methods produced closest agreement for current velocities of less than 40 cm/sec and with satellite-derived velocities obtained with sequential 12 hour images rather than sequential 24 hour images. Satellite-derived velocities in the rapid flow area (larger than 40 cm/sec) showed poor correspondence to DAL-measured velocities. The strong current shear in these areas may distort the surface SST patterns making identification of features between two images more difficult. The satellite derived surface velocities are assumed to be representative of the velocities of the upper mixed layer, which is usually 10 to 30 m deep in the study region.

TABLE OF CONTENTS

LIST OF FIGURES

ACKNOWLEDGEMENTS

The completion of this thesis was made possible by the generous assistance of many individuals. I would like to thank Ms. Melissa L. Ciandro and Mr. John F. O'Hara for supplying the satellite data set and for their instruction in utilizing the COMTAL imaging processing system. I am indebted to Dr. Philip A. Durkee, my co-advisor, for his programming assistance and remote sensing knowledge. Dr. Laurence C. Breaker's assistance in testing the vector generation program (OCEANTRAK) is also appreciated. Dr. David C. Smith's enthusiasm in dynamic oceanography greatly influenced me in selecting the topic and contributed to my own enthusiasm in conducting the study. I would like to thank Mr. Hsu for his invaluable support in image processing. Lt. Gail Griffin and Mr. Steve Blankschein assisted in the English composition of the final product. I would like to thank Mr. Craig Motell who assisted in the transfer of my satellite data to the Idea Lab. To my thesis co-advisor, Dr. Steve Ramp, I extend my deepest gratitude and appreciation for his continuing concern, guidance and support throughout the thesis process.

I. INTRODUCTION

The ocean is a complex system with movement and variability in the temporal and spatial dimensions. The ship, as the oceanographer's traditional measurement platform, can gather neither a long time series at a fixed point nor a synoptic chart at a fixed time. In spite of this mismatch of existing physical characteristics and limited sampling abilities, meaningful shipboard observations can be made through a vertical column of the ocean. Instrumented moorings and drifting buoys, developed relatively recently, are expensive to use and can cover only small areas of the ocean surface. Although the need to take measurements directly from the ocean to achieve a three-dimensional data set will remain, satellite remote sensing has revolutionized the gathering of oceanographic data. For example, satellite observations have been used to estimate large-scale surface variability of SST, plankton concentrations, and sea ice extent.

Satellite remote sensing has greatly contributed to our knowledge of the general circulation of the ocean, meso-scale eddies and upwelling, small frontal systems, and surface and internal waves. There remain, however, two major problems in exploiting remote sensing of the ocean:

1. Accurately and unambiguously assimilating the vast amount of data received from the satellite's sensor.
2. Relating the surface data to internal processes.

The recent development of more powerful image processing hardware has helped to compile the huge amounts of data, and has created the data sets necessary to this thesis.

One application of remote sensing is to use the displacement of SST features visually identified in sequential IR satellite images to estimate surface current velocities. Koblinsky et al. (1984) followed the 10-20 km SST features observed in Advanced Very High Resolution Radiometer (AVHRR) images to estimate the surface flow around a large California Current Eddy. La Violette (1984) estimated the average motion around the Alborean Sea gyre by noting displacements of SST features in sequential AVHRR infrared imagery. Vastano and Borders (1984) used a similar technique with an interactive computer display system to calculate surface flow from displacements of SST features in sequential images. Vastano and Reid (1985) used this subjective

technique, called feature tracking, to generate stream functions and sea surface topography approximations. O'Hara (1987) used unenhanced black and white AVHRR IR images to derive sea surface velocities using a feature tracking technique for an area off the Central Coast of California.

A feature tracking technique was used in this thesis to estimate sea surface velocities from 27 and 28 April 1981 AVHRR IR data for an area off the central coast of California. The area and period studied were chosen to coincide with O'Hara (1987) to allow direct comparison of the results. The primary assumption of the feature tracking technique used is that the displacement of SST features evident between the first and second images for a given interval are indicative of surface flow rates in that area. A color enhancement of SST gradients is performed on the AVHRR IR images to aid in visually identifying advecting SST features. The positions of the identified features in sequential IR images are recorded by an interactive computer program and display system. The computer program uses these positions to calculate and display surface flow components.

The content of this thesis is as follows: Chapter II presents background information on the general characteristics of the California Current System (CCS) within the research region. Chapter III presents the data. Chapter IV discusses the IR image enhancements applied to the data. Chapter V presents the following: 1) the satellite data processing and procedures used to load the data into the Naval Postgraduate School's COMTAL image processing system; 2) error analysis for the sea surface velocity measurements; 3) the Doppler acoustic log results;and 4) Comparisons of the vectors derived from this investigation to those derived by O'Hara (1987) and from the Doppler acoustic log (Kosro 1986). Chapter VI presents the conclusions for this study and lists some recommendations for further research.

II. THE CALIFORNIA CURRENT SYSTEM WITHIN THE RESEARCH REGION

A schematic drawing of the northeast Pacific circulation is shown in Figure 2.1. The California Current System (CCS) forms the eastern boundary of the great clockwise circulation of the North Pacific Ocean. At high latitudes, the water moves eastward under strong westerly winds, and divides into two branches near the coast of North America. A small part turns northward into the Gulf of Alaska, and the larger part turns southward, parallel to the coast of California. Beneath this flow and concentrated over the continental slope is a poleward flow know as the California Undercurrent. There is also a variable surface poleward flow near the coast, sometimes called the Davidson Current. These currents form the main structure of what is referred to as the California Current System (Van Dorn, 1974).

In general, the temperatures in the open ocean are colder further north, so that the northern branch is a relatively warm current while the California Current or southern branch is a relatively cold current when compared to the water farther offshore. As the latter drifts south, at speeds generally less than 25 cm/sec, it becomes warmer under the influence of solar heating and by mixing with offshore water (Reid et al., 1974). Near latitude 25°N, the California Current swings westward to join the North Equatorial Current. The California Current is characterized by several persistent local circulations inshore of its main drift, which stays 60 to 150 km off the coast. A small clockwise eddy is usually situated about 130 km off Cape Mendocino and a similar eddy persists between Guadalupe Island and the coast. Another permanent eddy, sometimes called the Southern California Countercurrent, is found to the south of the submerged peninsula that extends southwest from Point Conception to Cortez Bank and includes Santa Rosa and San Nicolas Island. The waters southeast of Point Conception are protected from the prevailing northwest winds and also from the southerly offshore currents. The currents here are weak and usually flow to the north. The water here remains off the coast of southern California for a considerable time and becomes much warmer than the water offshore, which is constantly replaced by cooler water from the north.

A deep countercurrent, below about 180 m, flows to the northeast along the coast from Baja California to past Cape Mendocino. Consequently, the California

Current refers to the surface equatorial flow; the California Undercurrent refers to subsurface poleward flow over the continental slope; and the Davidson Current refers to the surface poleward flow that occurs north of Point Conception during late fall and early winter (Hickey, 1979). The California Current system is of particular interest to oceanographers during the upwelling season which last from approximately March to July. The coastal upwelling season is a period of pronounced mesoscale changes in currents, temperatures, and salinities from the non-upwelling season.

The Coastal Ocean Dynamics Experiment or CODE (Beardsley and Lentz, 1987) was designed to identify and study those dynamical processes which govern the wind-driven motion of water over the continental shelf. Winds were strongly favorable for upwelling during the 1981 experiment. The surface temperature and salinity fields reflect the influence of both the seasonal winds and day-to-day variations in the wind. Persistently low surface salinities offshore reflect the general southward advection of local subarctic water, and the sporadic low salinities over the inner shelf reflect northward advection of local runoff through an intermittent narrow countercurrent along the coast. Circulation patterns imbedded in this region were very complex and included meandering equatorward flow, cyclonic and anticyclonic eddies, and the inshore countercurrent. Overall average fields were relatively simple showing a broad equatorward surface flow, a very weak inshore countercurrent, and a definite poleward undercurrent at the shelf break (Huyer and Kosro, 1987). Average isotherms and isohalines were not strictly parallel to coastline. South of the coastline bend at Point Arena, they gradually diverged from the coast.

Current estimates for CODE were obtained by filtering combined Doppler acoustic log (DAL) and navigation (LORAN-C) data over 30 minute intervals (Kosro, 1985). The DAL maps for the period studied in this thesis (26-28 April, 1981) do not show clear evidence of a continuous equatorward current although the dynamic topography observed during this survey indicated a meandering but rather weak (less than 20 cm/sec) baroclinic jet. Instead the survey shows the presence of one or more circular or elongated eddies. On the smaller scale, more confused, eddy like features were observed over the slope and the entire shelf during 26-28 April 1981, and these eddies seem to penetrate down to at least the 150 m level, considerably deeper than the coastal jet. A continuous inshore countercurrent was not observed during this survey (Huyer and Kosro, 1987).

In conclusion, the California Current System at the time of this study consisted of a weak meandering current intermingled with synoptic-mesoscale eddies. The across-shore currents induced by these features may account for the elongated, cool surface features that are sometimes observed extending across the California Current region in the satellite measured SST fields.

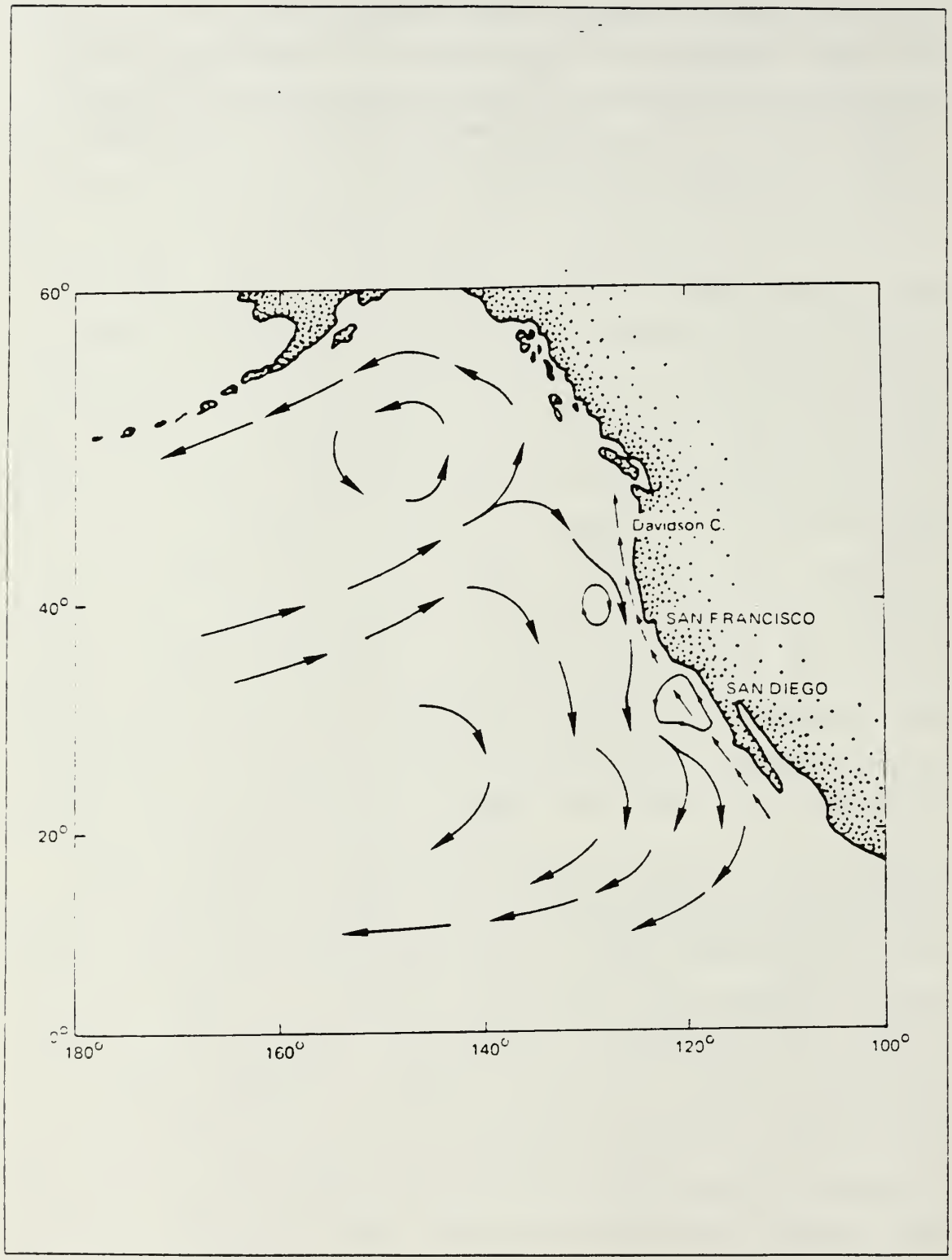

Figure 2.1 The large scale Circulation off Western North America (From Van Dorn, 1974).

III. DATA

A small portion (40 km wide, 100 km long) of the California Current System, (Figure 3.1), was selected for analysis in this thesis. Over this region NOAA-6 AVHRR digital satellite data from 27 April 1981 through 28 April 1981 were used in estimating coastal surface current velocities.

The digital satellite data consisted of three IR measurements and two visible measurements. The IR measurements were taken at 12 hour intervals for the following times: 16:15:00 GMT, April 27; 03:34:00 GMT, April 28; and 15:52:00 GMT, April 28. The visible measurements were taken at 16:15:00 GMT, April 27 and 15:52:00 GMT, April 28. Both the IR measurements taken from channel 4 (10.5-11.5 micrometer) and the visible measurements taken from channel 1 (0.58-0.68 micrometer) AVHRR data have a resolution of 1.1 km by 1.1 km at the subsatellite point.

The digital satellite image data used in this study were received and processed at Scripps Institute of Oceanography (SIO). The data were available from SIO in the form of 512 by 512 pixel (1.1 km pixels) arrays of visible and IR imagery for the region included in this study. Calibration and navigation of the satellite images were performed at SIO, but no correction was made for atmospheric water vapor contamination of the IR images. However, since relative SST features (gradients), rather than absolute SST features were used for the tracking process, and because the spatial distribution of atmospheric water vapor is generally much more uniform than the spatial distribution of SST gradients (Emery et al., 1986), SST gradients will appear weaker but their position will not be altered in the presence of atmospheric water vapor. Therefore, the influence of the water vapor on surface velocity estimates obtained here should be small.

The study region and period were chosen to coincide with the Coastal Ocean Dynamics Experiment (CODE). During CODE, current velocity profiles were obtained by means of an Ametec-Straza Doppler acoustic log (DAL). The DAL current profile data typically spanned a depth range of 15-150 m, with each measurement separated by 6.5 m. Current measurements were obtained by filtering the combined DAL and Navigation (LORAN-C) data over intervals of 30 minutes (Kosro, 1985). The accuracy of these shipboard current estimates can be judged from comparisons with

vector measuring current meters moored over the shelf and slope during CODE. These comparisons showed that the correlation between the shipboard and moored measurements were 0.95-0.97 for the energetic alongshore flow component and 0.76-0.82 for the weak cross-shore flow component (Kosro and Huyer, 1986), with a 5 cm sec standard deviation of the differences. (See the appendix for more information on DAL operation.)

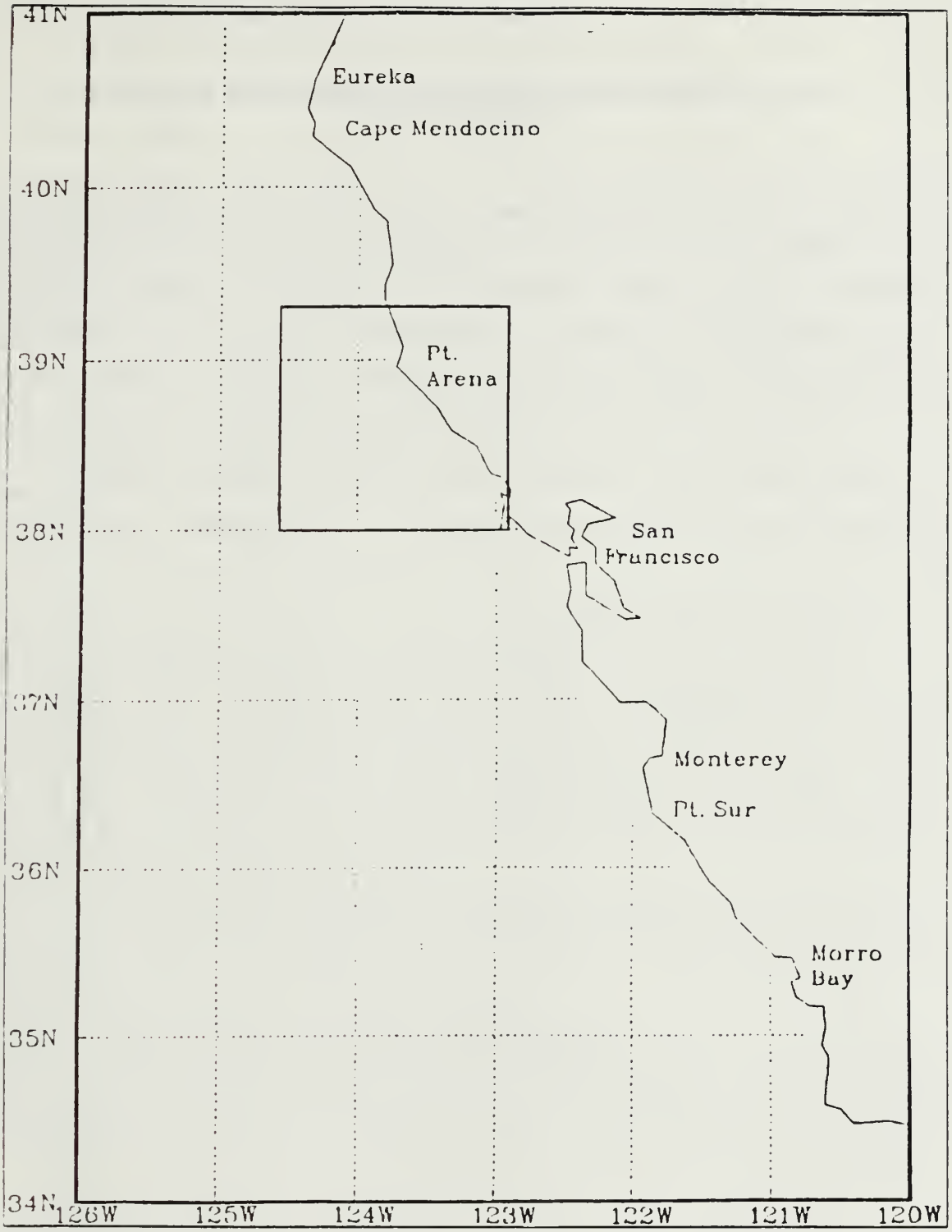

Figure 3.1 The central coast of California.
The study area is enclosed by the box.

IV. SATELLITE DATA PRE-PROCESSING AND IR IMAGE ENHANCEMENT

The feature tracking technique used in this thesis requires the visual identification of SST features on an interactive image display system. After these features are identified in sequential images, a computer algorithm, loaded on the display system, is used to calculate the displacement of these features. From this displacement, the computer algorithm calculates, stores, and displays the resultant current vectors. Unfortunately, the SST features are not always readily discernable to the analyst. Therefore, these features need to be enhanced to allow the analyst to detect and track the features. This chapter discusses the data processing, cloud identification, and image enhancement techniques used to make the SST features more apparent to the analyst.

A. CLOUD IDENTIFICATION

To begin processing, the AVHRR satellite data was loaded from magnetic tape into the Naval Postgraduate School (NPS) Computer Science's VAX 11/780. The VAX 11/780 computer is connected to a COMTAL Image processing system which is used for displaying and manipulating the satellite data. The two visible 512 by 512 pixel images, loaded on the VAX 11/780, were displayed on the COMTAL system and visually examined to determine the extent and location of any clouds which would contaminate the infrared signal received by the satellite. This procedure was done by O'Hara (1987) and was repeated in this study. All subsequent analyses were carried out on the IR data.

Visual inspection of the visible imagery (Figures 4.1 and 4.2) indicated only a small area of cloud cover in the study region. This area of cloud cover occurred in the northwestern corner of the study region on April 28, 1987 (Figure 4.2), and obtaining accurate current velocity estimates beneath this area of cloud cover was impossible. Some mid and high level thin clouds appearing in the IR imagery (Figure 4.4) but not in the visual imagery, would also affect the underlying current velocity estimates and these areas were left out of the analysis.

The original unenhanced Scripps satellite (NOAA-6) IR images are presented in Figures 4.3, 4.4 and 4.5. These IR images, taken approximately 12 hours apart, form the database used to derive surface current velocity estimates discussed in this thesis.

B. IMAGE ENHANCEMENT PROCEDURES

Before discussing the enhancement procedures applied to the data shown in Figures 4.3-4.5, a brief discussion of image enhancement principals is presented. The principal objective of enhancement techniques is to process a given image so that the resulting image is more suitable than the original image for a specific application. Image processing can be divided into two broad methods: the frequency-domain method and the spatial-domain method (Gonzalez, 1977). The frequency-domain method is based on modifying the Fourier transform of an image. The spatial-domain method, on the other hand, refers to the image plane itself, and is based on direct manipulation of the pixels in an image. One such spatial-domain approach is based on gray-level mapping of the pixel where the type of mapping used depends on the criterion chosen for enhancement.

When processing an image for visual interpretation using either of the above methods, the viewer is the ultimate judge of which method is better because, generally, there is no agreed upon "best method" of image processing. Visual evaluation of image quality is a highly subjective process, thus making the definition of a "best image" an elusive standard by which to compare algorithm performance; however, when the problem is one of processing images for feature tracking, the evaluation task is somewhat easier. If, for example, one were dealing with "discerning" a feature of sea surface temperature, the best image processing method would be the one yielding the best human recognition results. Because of the subjectivity of image processing, one is often faced with a certain amount of trial-and-error before being able to settle on a satisfying image processing approach.

After attempting several different image enhancement procedures, a combination of three image enhancement procedures produced a "best image" for SST feature tracking. These procedures are discussed below.

1. Image enhancement by histogram modification

The first procedure entailed image enhancement by histogram modification. A histogram of gray level content provides a global description of the appearance of an image. The enhancement histogram of a given image can be determined by selecting a probability density function to change the pixel values (0-255) in the image to new pixel values. The type and degree of enhancement obtained depends on the nature of the specified histogram. There are two methods to achieve the histogram enhancement; one is histogram equalization, the other is direct histogram specification.

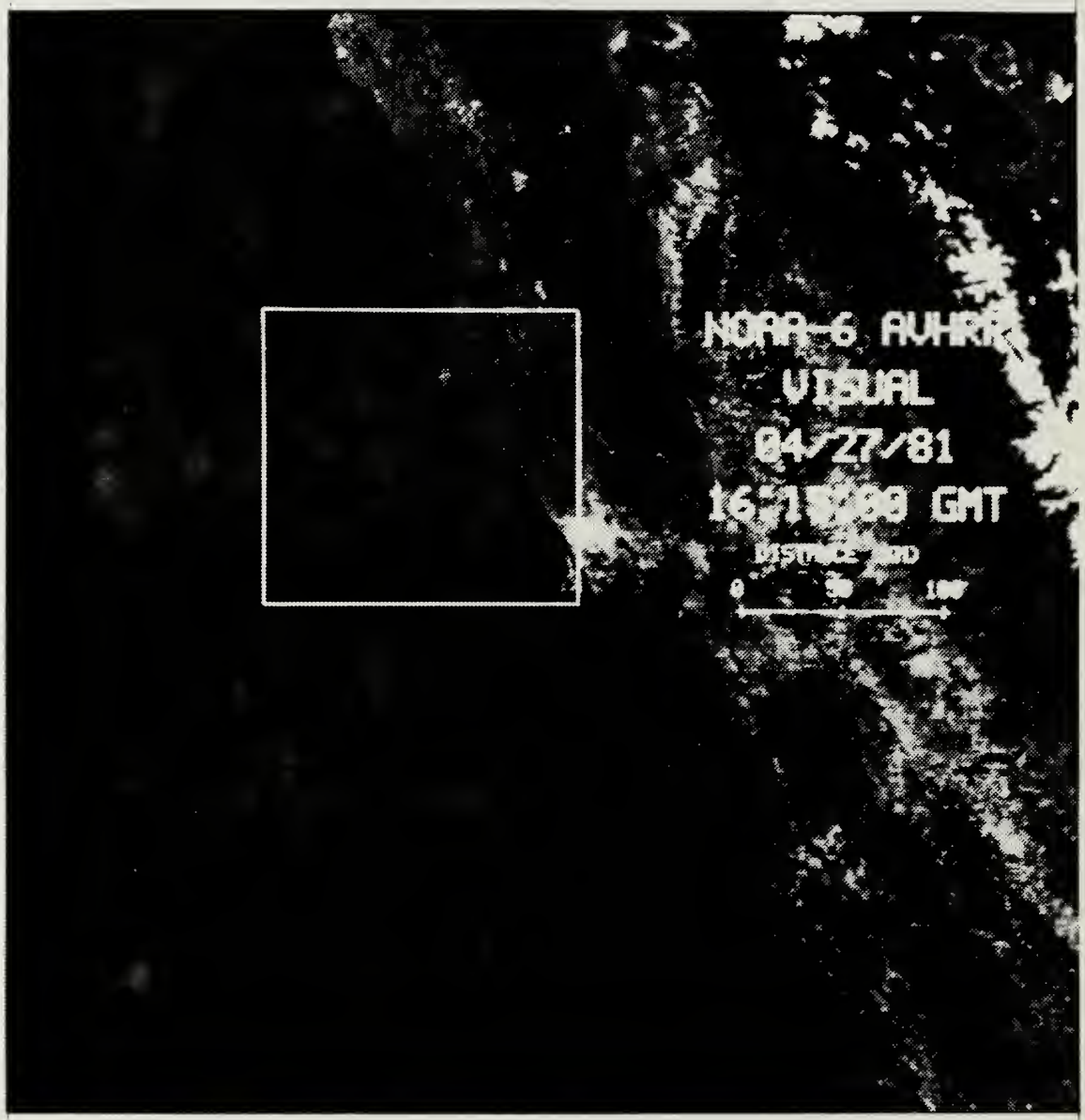

Figure 4.1 NOAA-6 AVHRR Visible image 04/27/81 16:15:00 GMT.

Figure 4.2 NOAA-6 AVHRR Visible image 04/28/81 15:52:00 GMT.

Figure 4.3 NOAA-6 AVHRR Infrared image 04/27/81 16:15:00GMT.

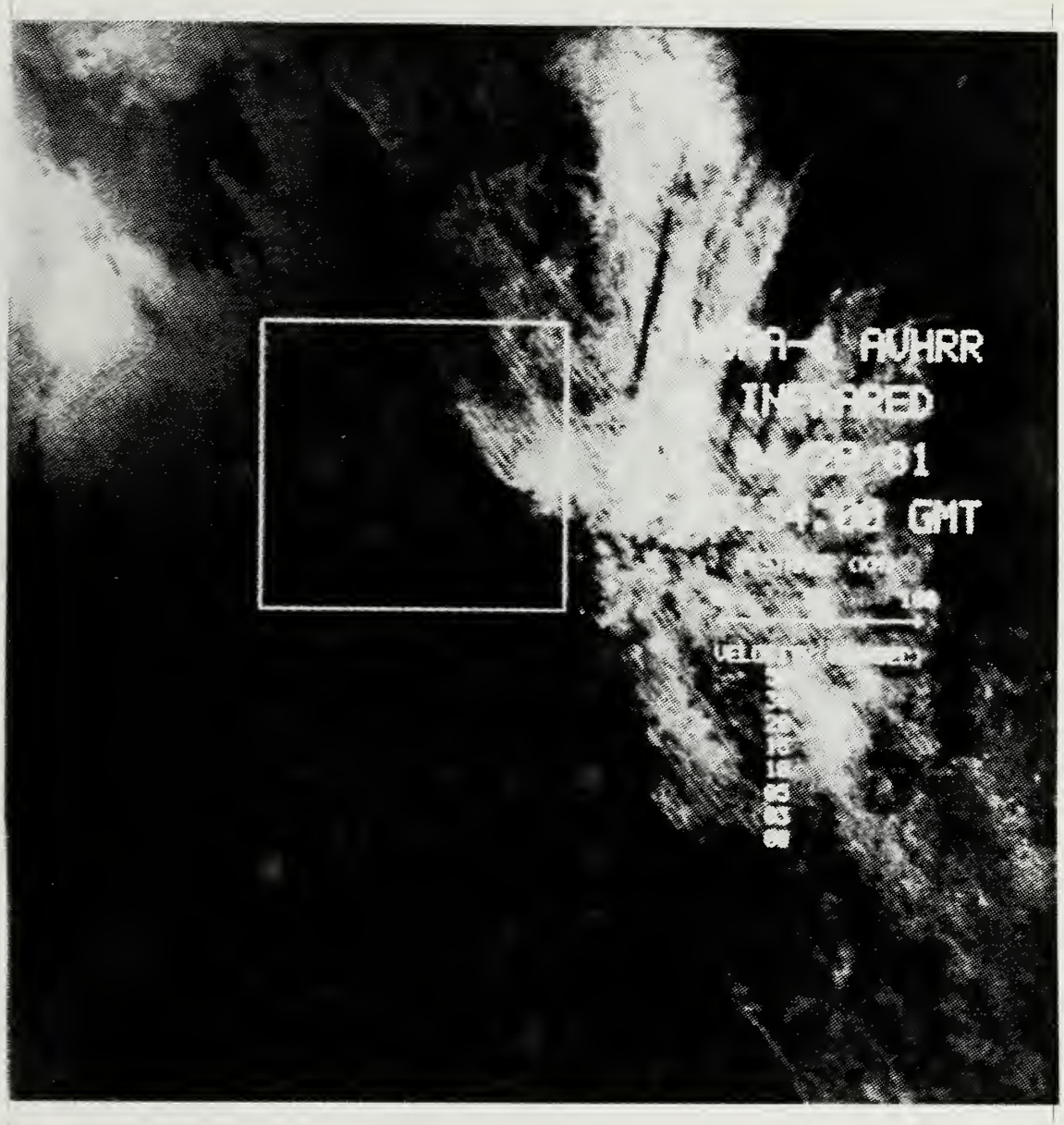

Figure 4.4 NOAA-6 AVHRR Infrared image 04/28/81 03:34:00GMT.

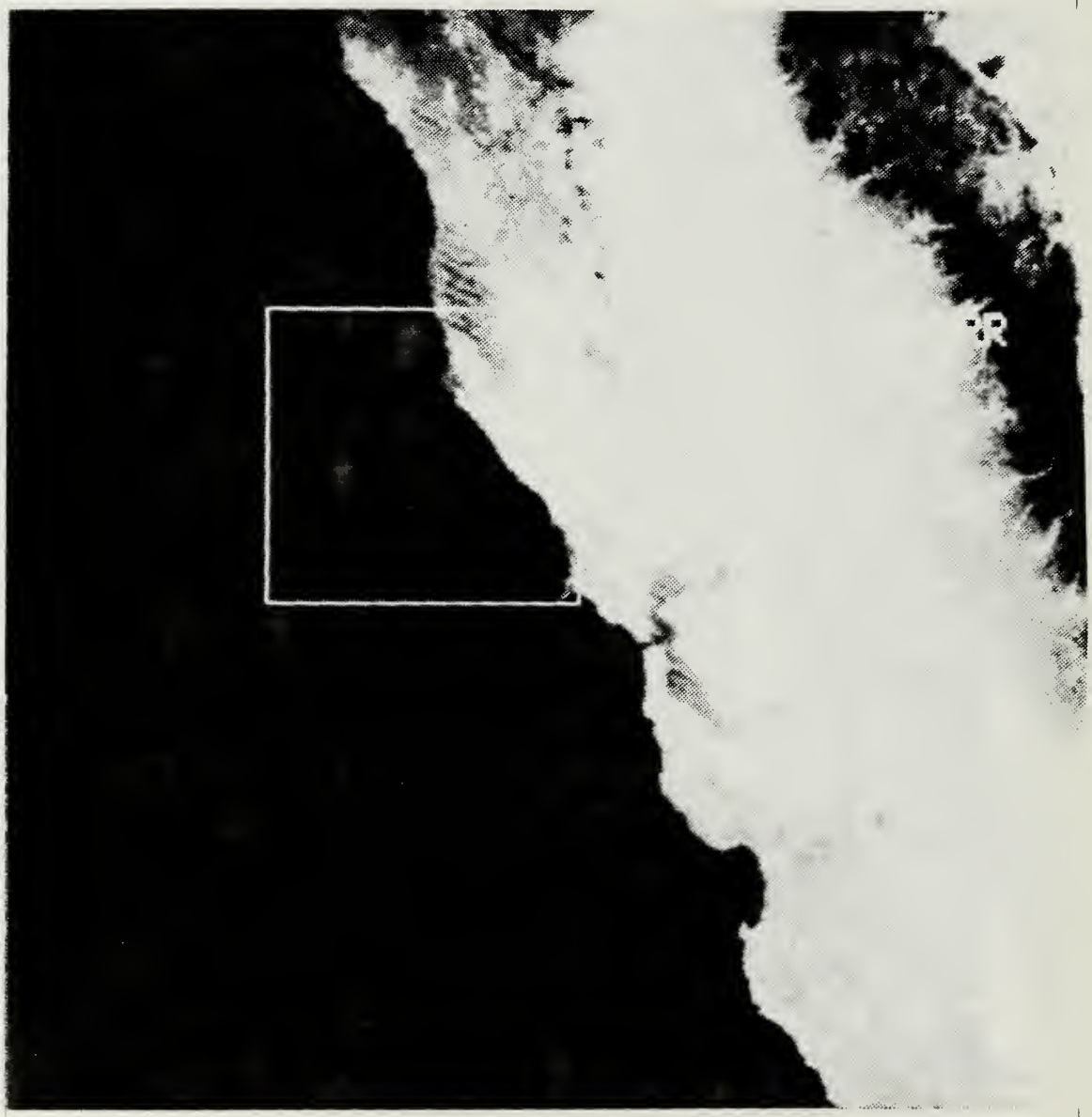

Figure 4.5 NOAA-6 AVHRR Infrared image 04/28/81 15:52:00GMT.

Software for both methods are available on the COMTAL system. Although the histogram equalization is quite useful, it does not lend itself to interactive image enhancement applications, because the capabilities of this method are limited to the generation of only one result--an approximation to a uniform histogram.

In this thesis the direct histogram specification method is used to specify interactively particular histograms capable of highlighting certain IR gray level or SST ranges in an image. The results of applying the direct histogram approach to Figures 4.3 - 4.5 are shown in Figures 4.6 - 4.8, respectively. The enhanced image features are similar to O'Hara's image features where a linear enhancement scheme was used. Still the boundaries between SST features in the resultant images are hard to discern.

2. **Image sharpening and smoothing**

The second procedure entailed image sharpening and smoothing. Sharpening methods are useful primarily as enhancement tools for highlighting feature edges. A sharpening method is used to enhance the feature boundaries of Figures 4.6-4.8, and thus, the ability of the analyst to interpret these edges. One technique for sharpening boundaries in an image is to use differentiation. The most commonly used method of differentiation in image processing applications is referred to as the gradient method. The gradient equation, developed and used in this thesis, is given in finite difference form by

$$\begin{aligned} G<f(x,y)> \;=\; & 1/8 \times \{|f(x+1,y-1)-f(x-1,y-1)| + |f(x+1,y)-f(x-1,y)| \\ & + |f(x,y+1)-f(x,y-1)| + |f(x+1,y+1)-f(x+1,y-1)| \\ & + |f(x+1,y+1)-f(x-1,y+1)| + |f(x-1,y+1)-f(x-1,y-1)| \\ & + |f(x+1,y+1)-f(x-1,y-1)| + |f(x-1,y+1)-f(x+1,y-1)|\} \end{aligned} \qquad \text{(eqn 4.1)}$$

where $G<f(x,y)>$ is the gradient magnitude, f(x,y) is the pixel gray value, x is the image element position (0-512), and y is the image scan line position (0-512). Note, that (eqn 4.1) approximates the derivative gradient by using differences, and it is always positive. The results of this equation can easily be calculated by computer. Since the magnitude of the gradient is proportional to the differences in gray levels between adjacent pixels, the gradient assumes relatively large values for prominent edges in an image feature and small values in regions that are fairly smooth.

While sharpening the edge of a feature has advantages, it also has disadvantages such as blurring the gradient in the interior of the feature. One solution

Figure 4.6 Histogram enhancement of
NOAA-6 AVHRR Infrared image 04/27/81 16:15:00 GMT.

Figure 4.7 Histogram enhancement of
NOAA-6 AVHRR Infrared image 04/28/81 03:34:00 GMT.

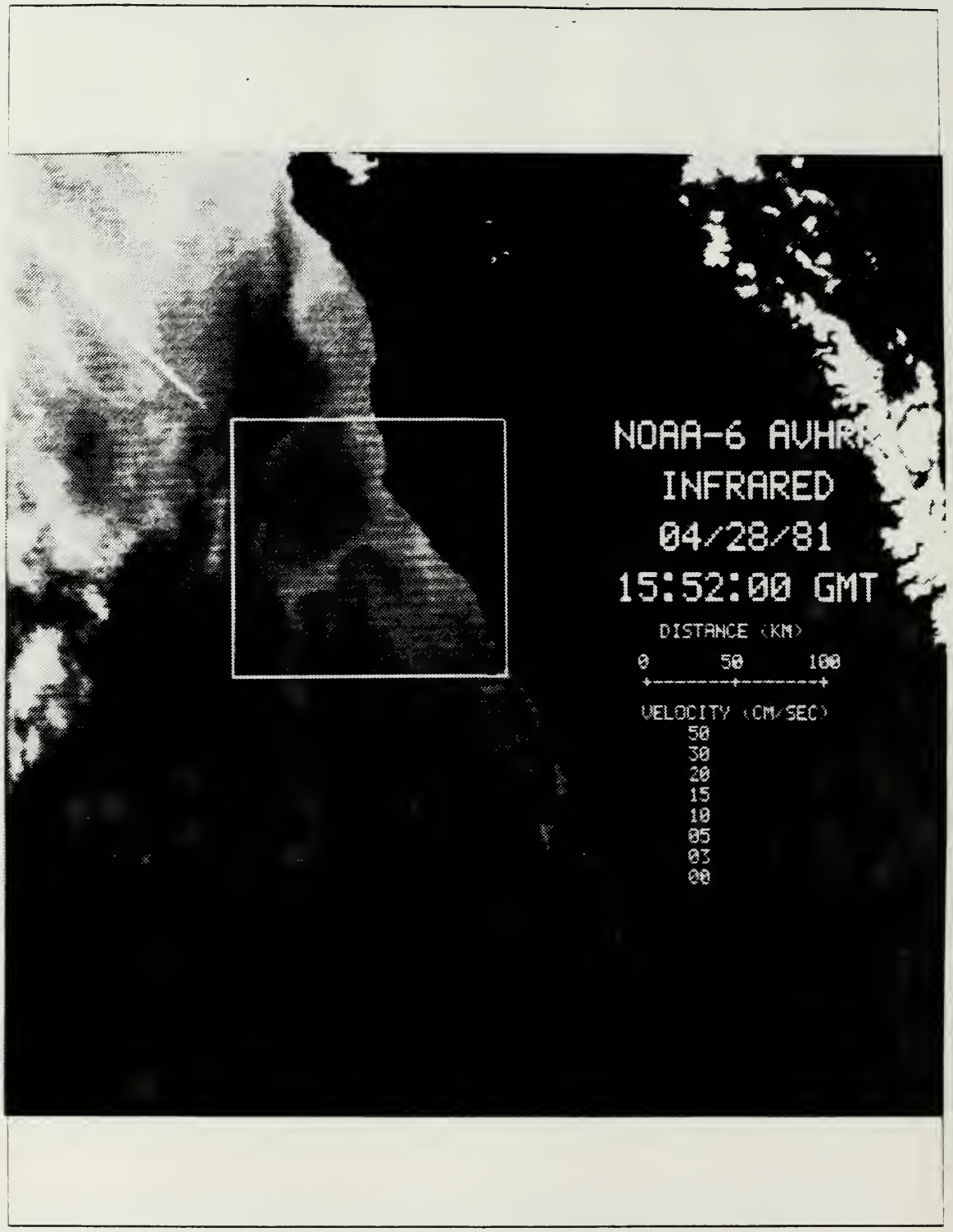

Figure 4.8 Histogram enhancement of
NOAA-6 AVHRR Infrared image 04/28/81 15:52:00 GMT.

to this problem, is to smooth the resultant gradient by dividing by a smoothing coefficient. The redefined "smooth" gradient function is given by:

$$M<f(x,y)> = G<f(x,y)>/S \qquad \text{(eqn 4.2)}$$

where S is the smoothing coefficient. The value of the smoothing coefficient was found by subjective trial-and-error testing and a smoothing coefficient equal to two was found to produce the best compromise between smoothing and sharpening of the SST features studied in this thesis.

The results of applying the gradient function, $M<f(x,y)>$, to the histogram images (Figures 4.6-4.8) are shown in Figures 4.9-4.11. Note how the smoothed gradient emphasizes the significant edges without destroying the characteristics of the smooth background.

3. **Pseudocolor enhancement technique**

The third and final procedure entails pseudocolor enhancement. The motivation for using color in image processing is that the human eye can discern more color shades and intensities than gray scale shades. In this research, the sharpened gray scale images (Figures 4.9- 4.11) were encoded into color images. Each pixel was mapped to a combination of red, blue and green intensities. The assigned pixel intensities were controlled by specifying the pseudocolor memory in the COMTAL system. After setting the pseudocolor memory, the pixel values in the gray scale images were mapped by the pseudocolor memories to a set of three color intensities and displayed on the CRT. This type of color coded image is referred to as a pseudocolor image. This kind of image allows one to differentiate minor gray scale differences which are not easily discernable on a black and white monitor. For this reason, a pseudocolor function memory was designed on the COMTAL system, and this memory was used to colorize the results of SST gradient enhanced images from Figures 4.9 through 4.11. The resultant images were used to trace "similar features" between these pseudocoloring images to yield sea surface current velocity estimates. The results of using the pseudocolor images with the feature tracking program are discussed in the following chapter.

Figure 4.9 Gradient enhancement of
NOAA-6 AVHRR Infrared image 04/27/81 16:15:00 GMT.

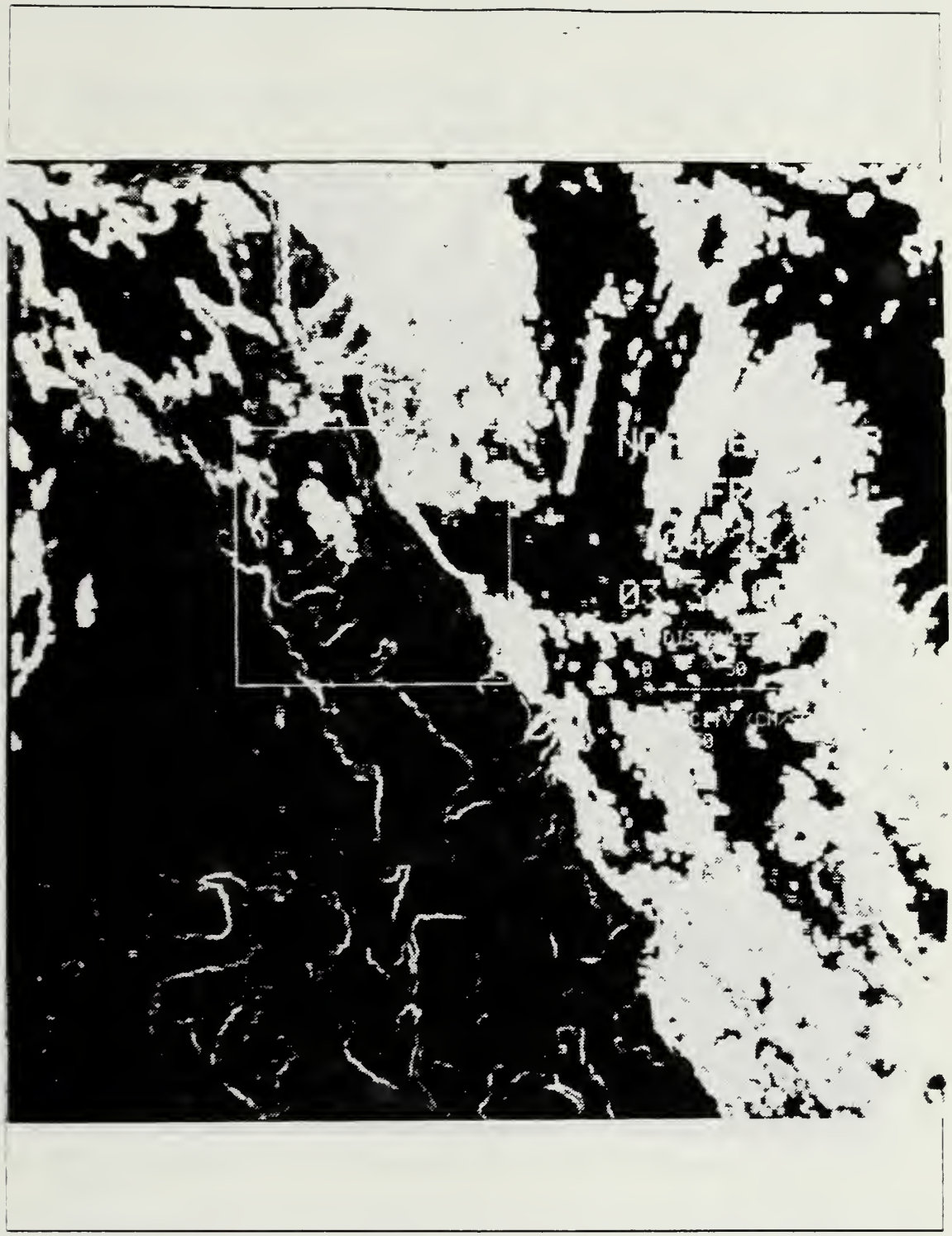

Figure 4.10 Gradient enhancement of
NOAA-6 AVHRR Infrared image 04/28/81 03:34:00 GMT.

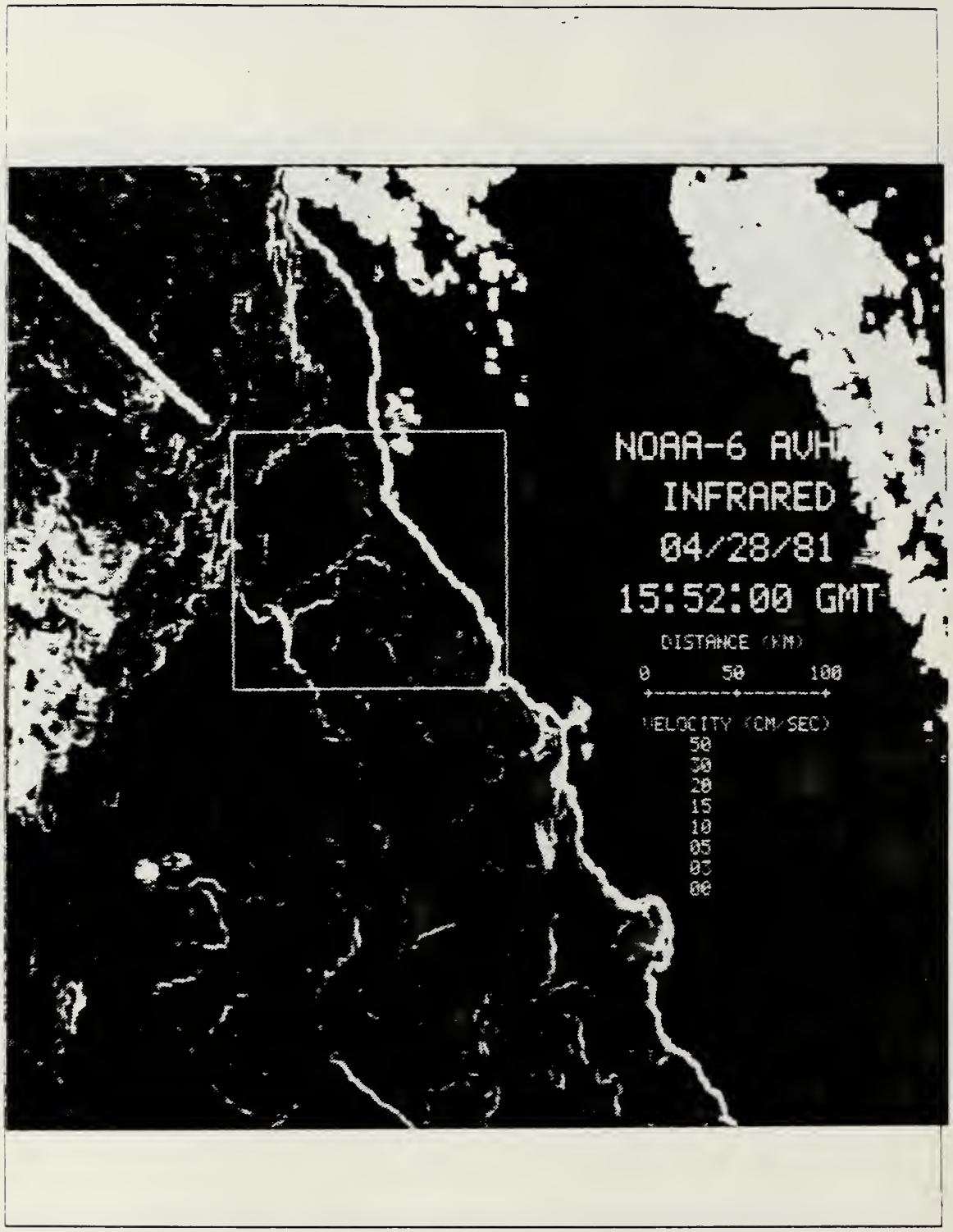

Figure 4.11 Gradient enhancement of
NOAA-6 AVHRR Infrared image 04/28/81 15:52:00 GMT.

V. CURRENT VELOCITY ESTIMATES USING FEATURE TRACKING TECHNIQUES

A. TRACKING THE SEA SURFACE CURRENT USING PROGRAM OCEANTRAK

After the enhancement of the AVHRR IR images, as described in Chapter IV, the resulting images were used to run a modified version of a cloud tracking program (developed by Michael Gunning of the NPS Meteorology Department and improved by O'Hara) that generates sea surface flow vectors from the displacement of identified surface patterns. With this interactive program, referred to as OCEANTRAK, individual flow vectors are generated by "marking" a feature in one image and then "toggling" to a second later image and "marking" the same feature again. This process was repeated as many times as necessary to track all the identified gradient features in the study area in both images. The OCEANTRAK program requires the user to input the time that the NOAA-6 sub-orbital track crosses San Francisco. This time is called the image crossing time. The first IR image crossed San Francisco at 16:15 on April 27, 1981, the second image at 03:34 on April 28, 1981, and the third image at 15:52 on April 28, 1981. The interval between the first and second images was 44340 seconds (12.32 hours), and the interval between the second and third images was 44280 seconds (12.30 hours). Because AVHRR data have a pixel resolution of 1.1 km, a scaling of cm p ps (centimeter per pixel per second) can be computed.

After loading the above information into the OCEANTRACK program, the following steps were performed on the COMTAL display system.

1. Enlarge the set of images which will be used to trace currents to two times the size of the original images. This step helps make the features more visible.
2. Overlay the research area in each set of images. This process reduced the navigation error between images and is referred to as the "Box Overlay Method" in this thesis.
3. Set the optimal pseudocolor memory function to determine the color of the images.
4. "Mark" a feature with a movable cursor on one image and then "toggle" to the second image and "mark" the same feature again.
5. Record the relative coordinate changes between the same features in both images, that is, the feature movement.

6. Once tracking is complete, reduce the set of images back to their original size, and collate all the coordinates that have been recorded in step (5) onto the original image set to compute the X and Y flow components.

The direction and speed of each feature track is determined by the number of pixels a feature moved in the east/west (X direction) and north/south (Y direction). After a feature was marked in each image, the resulting velocity vector was calculated and plotted onto the first graphics plane in the COMTAL display. These vectors are plotted midway between the feature's location on the first image and the feature's location on the second image. The vectors from each image are written into a temporary file which stores the position of the feature as well as the X and Y flow components. The resulting vectors are presented in Figures 5.1 and 5.2 and will be compared with the resultant DAL measured vectors shown in Figure 5.3 (from Huyer and Kosro, 1986).

B. VELOCITY MEASUREMENT ERROR

The two primary factors affecting the inherent accuracy of the tracking program OCEANTRAK are geographical location error of the AVHRR data and feature tracking error.

The geographical error results from image distortion, satellite time clock error, and the resolution of the data. Any inherent positioning error between the images will bias the velocity. A one pixel (1.1 km) shift between two images separated by 12 hours will result in velocity measurement uncertainties of 2.5 cm/sec (e.g. 1.1 km divided by 12 hours). After using the Box Overlay Method, image shift error was generally found to be less than 1 pixel, or less than 1.1 km. It is important to note, however, that the location of the area of interest in the satellite sensor data swath affects both position accuracy and data resolution. The AVHRR has an instantaneous field of view corresponding to a ground resolution of 1.1 by 1.1 km at nadir. The viewing geometry relative to the earth's curved surface causes this resolution to degrade to 2.5 by 1.1 km at the swath line edges (boundary area). Although the distortion can be corrected to a great extent by the Box overlay Method, data from the extreme edges of an overpass swath will clearly be of lesser quality. The data used in this thesis are located near the center of the swath so that the above problem can be neglected.

The tracking error is related to the precision with which the analyst is able to follow each tracked feature through the image series: the calculation of the displacement of features from one image to the next. While the tracked features have

dimensions of 2 to 5 pixels, the analyst generally tries to track a subportion of the feature (e.g. the leading edge, coldest/warmest part, etc.). Theoretically this would allow tracking the same spot in the thermal field to within one pixel accuracy. Unfortunately, the tracked features tend to change shape and intensity between images, and locating the same spot to within one pixel is often difficult. Obviously, the shorter the time interval between images, the more similar the features will appear; however, the severity of the error due to image misregistration or tracking problems increases at shorter time intervals. Minimal procedural error can thus be expected when using two images separated by the longest time period which still allows one to two pixel feature tracking accuracy. For this reason it is advantageous to know how long the trackable features preserve their identity. If a shorter time interval, like 6 hours, was available, a test could be performed to identify the average time that a feature can be identified. Because shorter intervals were not available, a 12 hour interval was used in the highly dynamic area being studied.

C. COMPARISON OF SATELLITE-DERIVED SEA SURFACE VELOCITIES TO 20 M DAL MEASURED VELOCITIES

The DAL current measurements, taken during CODE, were used to verify the satellite-derived current velocities. In order to objectively compare the DAL and satellite-derived velocities, a trackable feature should exist at the same time and location as the DAL track. With the data sets used in this research these conditions could never be met exactly, but they were approached as closely as possible while still allowing enough velocity data pairs for comparisons. From the first pair of images (16:15 April 27-03:34 April 28) there were 33 trackable features producing 33 current velocity estimates. From the second pair of images (03:34 April 28-15:52 April 28) there were 20 trackable features producing 20 current velocity estimates. O'Hara (1987) found 19 trackable features in the first set and 10 trackable features in the second set. Only 11 vectors were co-located with 20 m DAL measured vectors. This study obtained more vectors with greater confidence than O'Hara (1987). The direction of the vectors in both studies are consistent with each other, but the magnitude of the vectors in this study are slightly less than O'Hara's results.

The first set of vectors (Figure 5.1) show two groups of currents separated by a strong offshore current whose maximum current was about 25 cm/sec. The more northerly circulation appears to be an anticyclonic eddy. The other more southerly group of vectors flowed parallel to the coast and then turned offshore north of Point Reyes, forming another anticyclonic eddy.

The second set of vectors (Figure 5.2) had a stronger current over the offshore region (some vectors were greater than 50 cm/sec), and always flowed to the south except for two vectors at the northwest edge of the study area.

Using Point Arena (38°57'N, 123°44'W) as a landmark, (pixel coordinate 195, 156), the magnitude and direction of the 33 resulting vectors from the first pair of images were transfered to a geometrical map (Figure 5.4) and overlayed with the 20 m depth DAL vectors (Figure 5.5). Figure 5.5 shows only 12 co-located satellite-derived and DAL measured current vectors, and thus, the comparison is limited.

The direction of satellite-derived and DAL-measured currents are compared in Figure 5.6. The direction correspondence is such that 9 out of 12 pairs are within 45° of each other. The magnitude of satellite-derived and DAL measured currents are compared in Figure 5.7. The DAL-measured currents are always greater than the satellite-derived currents. For current magnitudes less than 25 cm/sec (as indicated by DAL measurements), the DAL magnitudes are approximately 2 times greater than the satellite-derived currents. For DAL measurements exceeding 25 cm/sec, the satellite-derived magnitudes are greatly underestimated and poorly correlated to DAL current magnitudes. Kelly (1983) also found that satellite-derived velocities were generally less than DAL measured velocities in an upwelling jet.

The velocity underestimation in the satellite measurements may be due to:

1. The problem of finding and accurately tracking features in regions of intense flow. In the present research the DAL experienced very high displacement rates when moving along sharp thermal gradients or within intense upwelling plumes. There are generally very few distinct trackable features in such regions and those that exist tend to disintegrate very rapidly.
2. Along a sharp boundary, barotropic shear instabilities often exist (Flament et al., 1985) which can be tracked rather easily, but do not represent the mean flow. Therefore, the tracking procedure may tend to track the instabilities and not the mean flow velocities.
3. The DAL results of Kosro (1985) showed that within a cold water jet, maximum velocity occurs some distance away from the frontal boundary. By tracking features at the front, the tracking algorithm will systematically undersample the region of highest velocity (as seen in Figure 5.7).
4. Differences between the current measurements from the two methods may also be related to the time scales involved in the data acquisition. The current estimates from the satellite data are derived from the displacement of features 12 hours apart and represent 12 hour averages; while the current estimates from shipboard DAL measurements represent 30 minute averages. Thus, relatively rapid fluctuations (less than 12 hours) in current velocities will result in different velocity estimates from the two methods.

5. Error introduced in the data itself, such as IR image contamination from clouds. For example, in the middle of Figure 5.5 the DAL-derived velocity was about 50 cm/sec, while in same area the satellite-derived velocity was 5 cm/sec. High and mid level clouds probably distorted the IR signal and caused this error (see the middle of Figure 4.7).

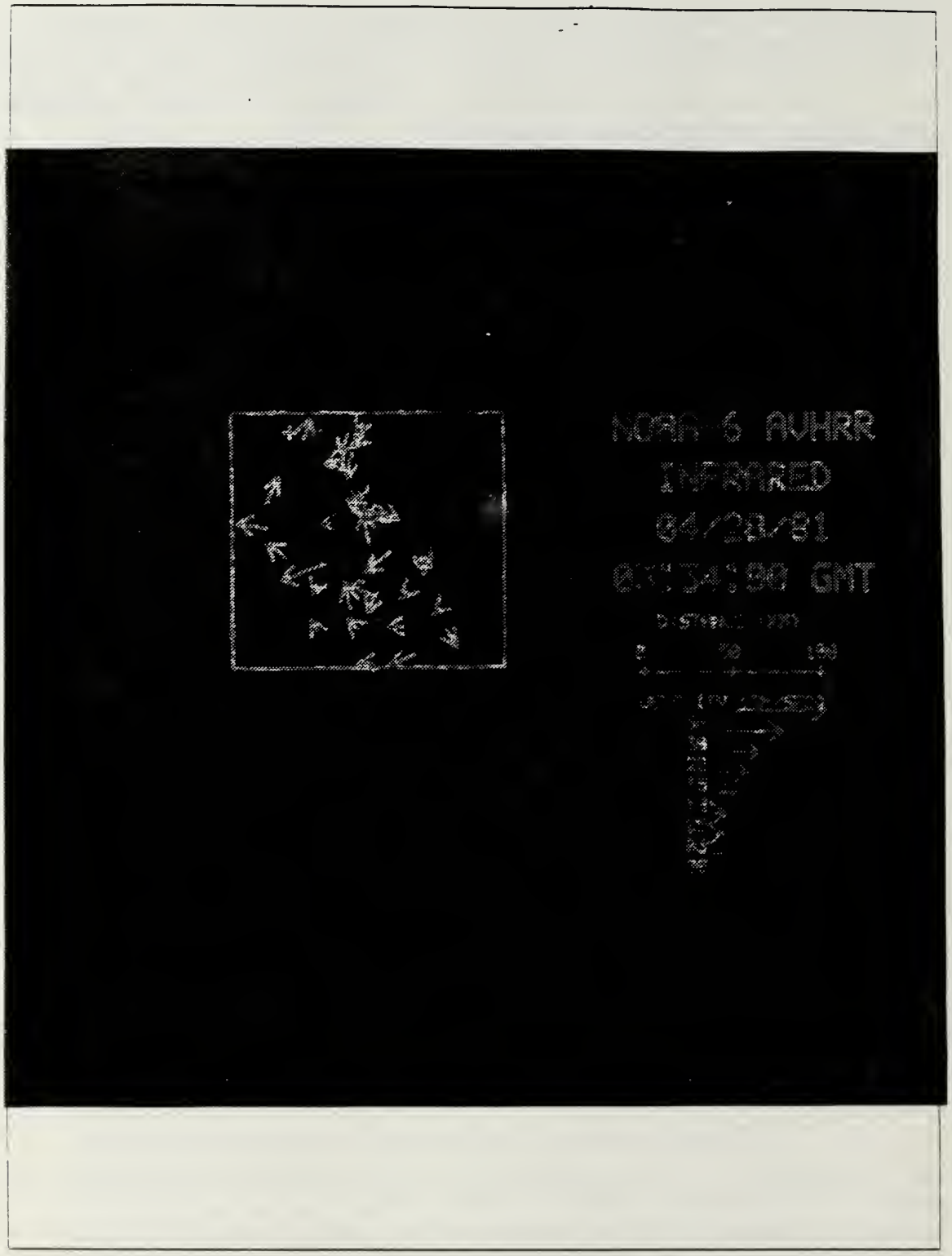

Figure 5.1 The first set of satellite-derived velocity vectors.

Figure 5.2 The second set of satellite-derived velocity vectors.

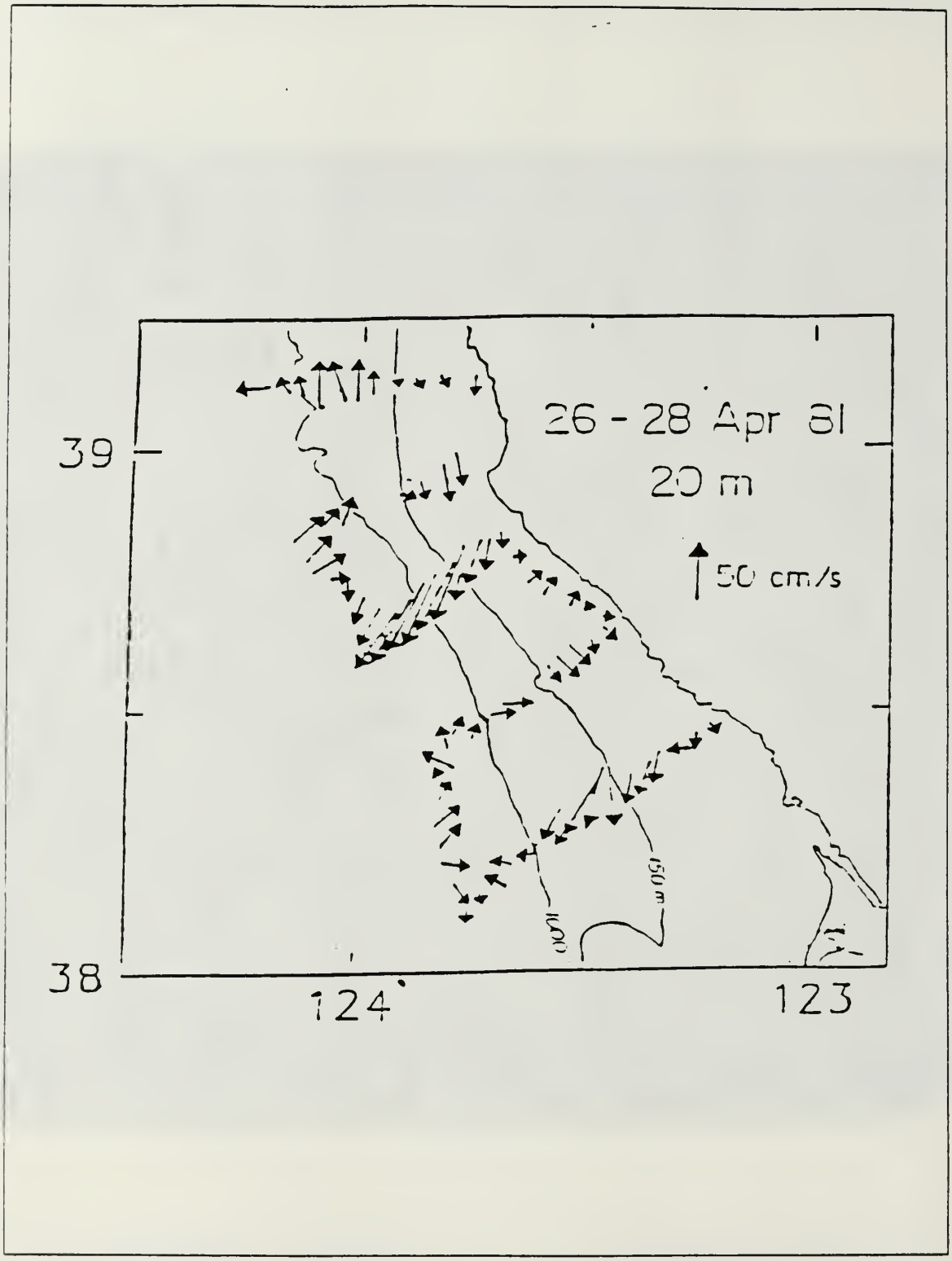

Figure 5.3 The DAL 20 m depth velocity vectors.

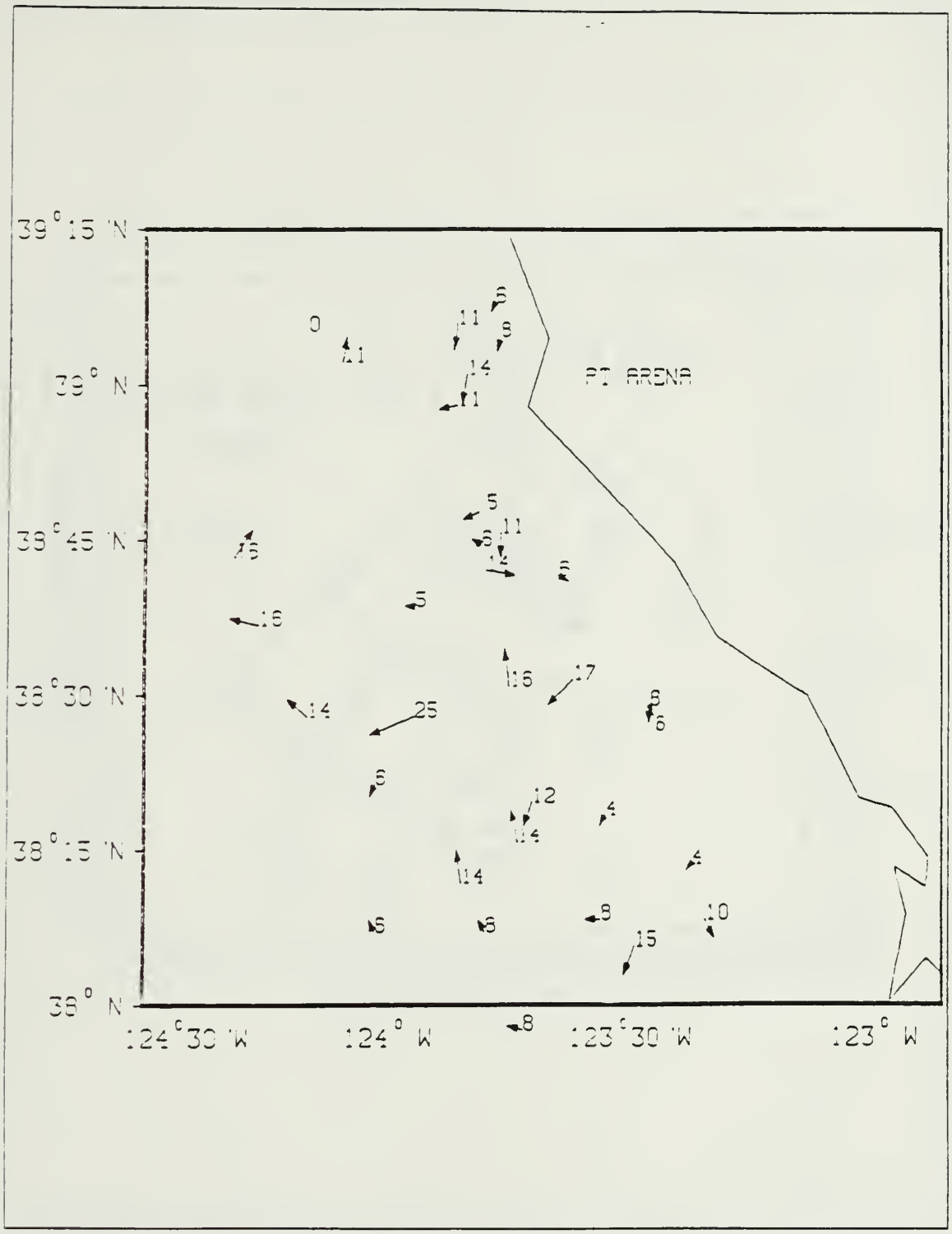

Figure 5.4 Satellite-derived velocity vectors from the first pair of images mapped onto a latitude-longitude scale.

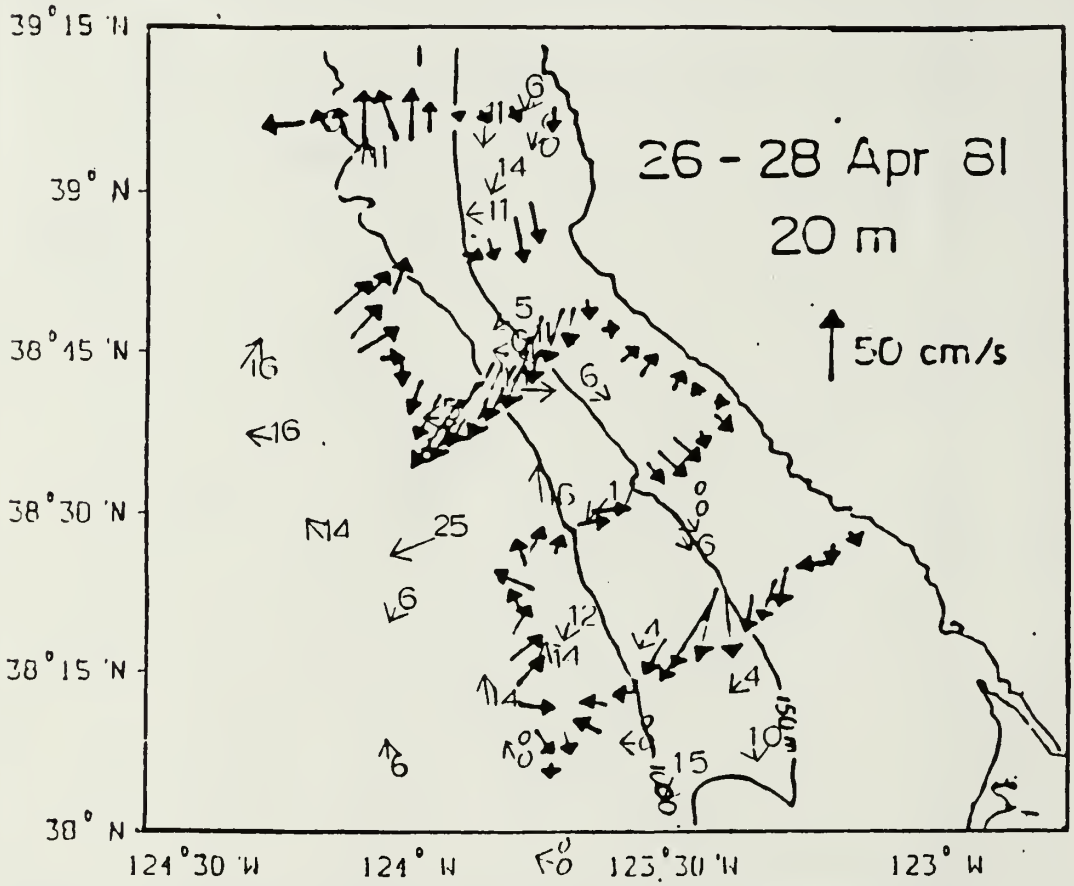

Figure 5.5 The comparisons between satellite-derived vectors (thin line) and 20 m depth DAL measured vectors (heavy line).

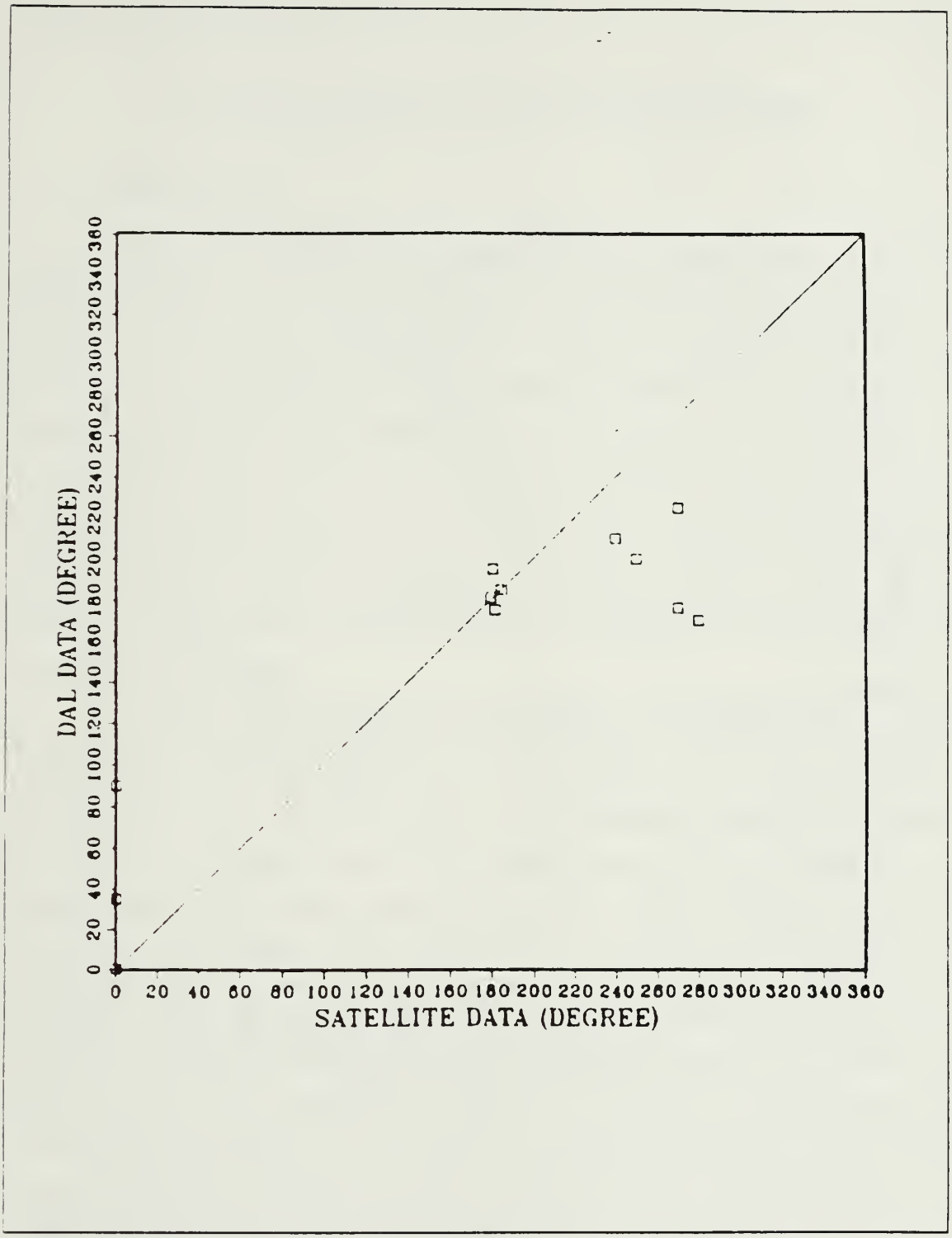

Figure 5.6 A comparison between satellite-derived and DAL-measured current direction.

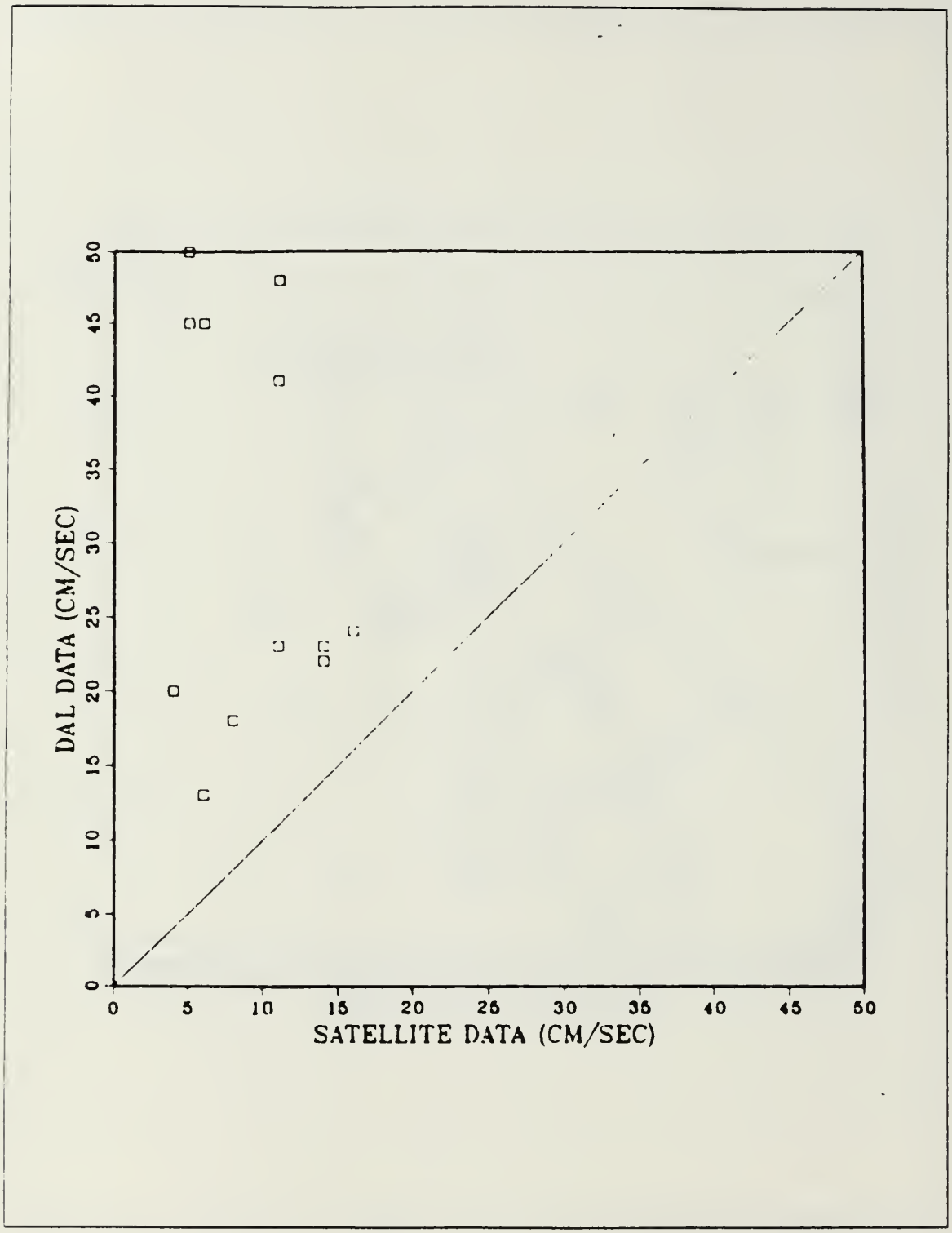

Figure 5.7 A comparison between satellite-derived and DAL-measured current magnitudes.

VI. CONCLUSIONS AND RECOMMENDATIONS

A. CONCLUSIONS

A technique for estimating surface current velocities from enhanced AVHRR infrared imagery was described. This technique was used to calculate the current flow field (near Point Arena) along the California coast. The direction component of the satellite-derived velocities compared well with the DAL measured current velocities. However, the satellite-derived velocity magnitudes always underestimate the DAL results. For DAL velocity magnitudes less than 25 cm/sec the underestimation is approximately linear. More data is necessary to determine if the satellite-derived velocities can be related to the DAL velocities with speeds greater than 25 cm/sec. These enhancement techniques improve feature tracking ability by obtaining nearly 50% more vectors than were obtained using unenhanced gray scale imagery (O'Hara, 1987). In addition, the velocities derived here are considered to be more accurate than those derived by O'Hara.

At present, feature tracking is the only method for providing comprehensive and truly synoptic flow field information over areas from a few hundred to thousands of square kilometers. Obtaining current measurements from satellite images is substantially cheaper for the user than using ground-based measurements and allows the monitoring of remote areas. The technique can be used to obtain up-to-date information or to calculate current profiles from archived imagery (as has been performed in this thesis). When coupled with in situ data, a fairly high resolution flow field can usually be obtained by taking into account the boundary locations of the different water types and the measured velocity gradients between them. This is a significant advantage over constructing a flow field from isolated measurements made with current meters or geostrophic calculations, which allow only blind interpolation between station positions. The nature of the technique requires a cloudless atmosphere and the existance of suitable features for tracking. Therefore, monitoring surface flow from AVHRR images is possible only in regions with heterogenous mesoscale surface features producing strong temperature gradients, such as off the west coast of North America.

In some areas such as the north Pacific gyre, the surface features may be too homogeneous to allow utilization of this technique. The trackable features must also preserve their identity from one image to the next. The extent to which the features preserve their shape greatly affects tracking precision and hence the accuracy of the measurements. Clearly, the closer in time the two images are recorded, the less the features will have changed, but the error due to imprecise tracking increases as the time separating the two images decreases. During this research, a 12 hour image-to-image time interval was found to be preferable to a 24 hour image-to-image time interval in minimizing tracking error. It was shown that satellite-derived measurements tend to underestimate surface flow in regions of very strong current and along sharp frontal boundaries. In such regions, small features within the current stream lose their identity too rapidly to allow accurate tracking. Other times the obtained vectors may result from tracking other persistent features, e.g. shear instabilities in the frontal boundary or periodic waves, whose propagation speed may not equal the true local flow velocity. Based on a limited amount of subsurface data, the directional component of the satellite-derived surface velocity was representative of at least the upper 10 m.

The measurement of small feature displacements in AVHRR IR images is a potentially efficient and economical means for obtaining sea surface flow velocities. Testing under various oceanographic and atmospheric conditions is needed to determine its general utility.

B. RECOMMENDATIONS

The accuracy of this technique is affected by image quality, feature stability, the time interval between images and tracking experience. The accuracy of the satellite-derived vectors can, nevertheless, be improved by the following !

1. Choose data from a later satellite (NOAA-7 or newer) with channels for a proper atmospheric correction. This can avoid shifts between images due to water vapor decrease or increase between images.
2. Remove human subjectivity by using an objective correlation scheme to track the features by computer.
3. Perform the research in different areas, seasons and atmospheric conditions, to assess these affects on the resulting vectors.
4. Use a repeatability test to examine the uncertainty introduced by subjective judgement in selecting the displacement of the same surface temperature feature on an image.

5. Use the Coastal Zone Color Scanner (CZCS) visible images to track ocean color features. Under most circumstances, ocean color will change less between images than SST does, which eliminates one source of error.
6. Obtain data from two polar orbiting satellites in order to decrease the time between satellite passes to 6 hours.

Finally, a combination of satellite data and in situ measurements would undoubtedly improve the estimates, since the in situ velocity measurements could be used to calibrate the satellite estimates. Although the resulting magnitudes may be too low, they could be used to test models of the surface velocity field, such as the assumption of horizontal non-divergence or upwelling along a front.

APPENDIX
DOPPLER ACOUSTIC LOG (TAKEN FROM KOSRO, 1986)

The shipboard Doppler acoustic log to be discussed here is a new tool for the measurement of ocean currents (Kosro, 1986). By providing vertical profiles of horizontal currents over the upper 150 m depth at points along the ship's path, it allows the ocean to be sampled in a way which is fundamentally different from moored current meters or drifters, which are the instruments most commonly used for current measurements. Consider the general problem of measuring the current as a function of time at a water parcel whose coordinates are $X_w(t)$ using an instrument whose location is $X_o(t)$. By a simple identity (as seen in eqn A.1).

$$dX_w/dt = dX_o/dt + d(X_w - X_o)/dt \qquad \text{(eqn A.1)}$$

Equation A.1 may be rewritten as A.2

$$u(X_o + r) = dX_o/dt + V(r) \qquad \text{(eqn A.2)}$$

The current u at the measurement point $(X_o + r)$ must be determined from the sum of two terms, where r is the distance between instrument and water parcel. The relative velocity V(r), is the velocity of the water parcel relative to the instrument position. The other, dX_o/dt, is the velocity of the instrument itself with respect to the Earth. Moored instruments and drifters each measure only one of these terms, and are engineered to make the unmeasured term, dX_o/dt for moored instruments and V(r) for drifters, negligible.

This design constraint places limits upon the types of variability which each instrument can sample. Although ocean currents vary in all three spatial dimensions as well as in time, a moored instrument samples only the temporal variability at a single location, while a drifter samples the time and space variablity only along the path of a single water parcel. For an instrument such as the DAL, which directly measures both V(r) and dX_o/dt, these constraints on possible sampling trajectories are removed. The speed with which the instrument can sample different locations becomes the new, less restrictive constraint on the set of (X,Y,Z,t) points which can be surveyed.

LIST OF REFERENCES

Beardsley R. C. and Lentz S. J., 1987: The Coastal Ocean Dynamics Experiment Collection : An Introduction. *J. Geophys. Res.*, **92, No. C2,** 1455-1463, Feb. 15, 1987.

Flament P., L. Armi and L. Washburn, 1985: The evolving structure of an upwelling filament. *J. Geophys. Res.*, **90,** 11765-11778.

Gonzalez, R. C. 1977: Digital Image Processing. Addision-Wesley Publishing Company, Advanced Book Program/World Science Division Reading, Massachusetts 01867 , U.S.A.

Hickey, B. M., 1979: The California current system-hypotheses and facts. *Prog. in Oceanog.*, **8,** 191-279.

Huyer, A., and P. M. Kosro, 1987: Mesoscale surveys over the shelf and slope in the upwelling region near Pt. Arena, California. *J. Geophys. Res.*, **92,** 1655-1681.

Kelly, K. A., 1983: Swirls and plumes or application of statistical methods to satellite-derived sea surface temperatures, Ph.D. thesis. *SIO Ref. 83-15, CODE Tech. Rep. 18*, Scripps Inst. Oceanogr., La Jolla, CA, 210 pp.

Koblinsky, C.J., J. J. Simpson, and T. D. Dickey, 1984: An offshore eddy in the California Current System, 2, Surface manifestation, *Progr. Oceanogr.*, **13,** 51-69.

Kosro, P. M., 1985: Shipboard acoustic current profiling during the coastal ocean dynamics experiment. *SIO Ref. 85-8*, Scripps Inst. Oceanogr., La Jolla, CA, 119 pp.

_____, and A. Huyer, 1986: CTD and velocity surveys of seaward jets off northern California, July 1981 and 1982. *J. Geophys. Res.*, **91,** 7680-7690.

La Violette, P. E., 1984: The advection of submesoscale thermal features in the Alborean Sea Gyre. *J. Phys. Oceanogr.*, **14,** 550-565.

O'Hara, J. F. March 1987: A Comparison of Satellite-Derived Ocean velocities with observations in the California Coastal Region. Masters thesis, Naval Postgraduate School, monterey, CA., 40 pp.

Reid, J. L., Roden, G. I., and Wyllie, J. G., 1958: Studies of the California Current System. *Califo. Coop. Oceanic Fish. Invest.* Rep. 5, 28-57.

Van Dorn, W. G., 1974: Oceanography and Seamanship. Dodd, Mead & Company New York, Library of Congress Catalog Card Number: 73-15377

Vastano, A. C., and S. E. Borders, 1984: Sea surface motion over an anticyclonic eddy on the Oyashio Front. Remote Sens. Environ., **16,** 87-90.

Vastano, A. C., and R. O. Reid, 1985: Sea surface topography estimation with infrared satellite imagery. *J. Atmos. Ocean. Tech.*, **2**, 393-400.

INITIAL DISTRIBUTION LIST

		No. Copies
1.	Defense Technical Information Center Cameron Station Alexandria, VA 22304-6145	2
2.	Library, Code 0142 Naval Postgraduate School Monterey, CA 93943-5002	2
3.	Chairman (Code 68Co) Department of Oceanography Naval Postgraduate School Monterey, CA 93943-5000	1
4.	Fang, Chung-ming Chinese Naval Hydrographic & Oceanographic Office Tsoying, Kaohsiung Taiwan 813 Republic of China	1
5.	Professor Steve Ramp, (Code 68Ra) Department of Oceanography Naval Postgraduate School Monterey, CA 93943-5000	1
6.	Professor Phillip A. Durkee, (Code 63De) Department of Meteorology Naval Postgraduate School Monterey, CA 93943-5000	2
7.	Professor David C. Smith, IV (Code 68Si) Department of Oceanography Naval Postgraduate School Monterey, CA 93943-5000	1
8.	Dr. Yao, Neng-Chun Chinese Naval Hydrogrpahic & Oceanographic Office Tsoying, Kaohsiung Taiwan 813 Republic of China	1
9.	Dr. Jeffrey Nystuen (Code 68Ny) Department of Oceanography Naval Postgraduate School Monterey, CA 93943-5000	1
10.	Commanding Officer Naval Ocean Research and Development Activity NSTL Station Bay St. Louis, MS 39522	1
11.	Commanding Officer Naval Oceanographic Office NSTL Station Bay St. Louis, MS 39522	1
12.	Commanding Officer Naval Environmental Prediction Facility Monterey, CA 93943	1
13.	Commander Naval Oceanography Command NSTL Station Bay St. Louis, MS 39522	1

14.	Officer in Charge Naval Oceanography Command Detachment Naval Air Station Moffett Field, CA 94035	1
15.	Oceanographic Section Chinese Naval Hydrographic & Oceanographic Office Tsoying, Kaohsiung Taiwan 813 Republic of China	3
16.	Kuo, Feng-Yu Chinese Naval Hydrographic & Oceanographic Office Tsoying, Kaohsiung Taiwan 813 Republic of China	1
17.	Craig E. Motell Department of Meteorology Naval Postgraduate School Box 63-ML Monterey, CA 93943-500	1
18.	LCDR G. R. Lennon Deck Department USS Dwight D. Eisenhower (CVN-69) FPO New York, NY 09532-2830	1
19.	Dr. Robert Beardsley Woods Hole Oceanographic Institution Woods Hole, MA 02543	1
20.	Dr. Mike Kosro College of Oceanography Oregon State University Corvallis, Oregon 97331	1